Binding Energies of the Silver Ion to Alcohols and Amides: A Theoretical and Experimental Study

Vladimir Romanov,[†] Chi-Kit Siu,[†] Udo H. Verkerk,[†] Houssain El Aribi,[‡] Alan C. Hopkinson,[†] and K. W. Michael Siu*,[†]

Department of Chemistry and Centre for Research in Mass Spectrometry, York University, 4700 Keele Street, Toronto, Ontario, Canada M3J 1P3, and MDS Analytical Technologies, 71 Four Valley Drive, Concord, Ontario, Canada L4K 4V8

Received: June 24, 2008; Revised Manuscript Received: August 22, 2008

The silver ion binding energies to alcohols (methanol, ethanol, *n*-propanol, *i*-propanol, and *n*-butanol) and to amides (acetamide, *N*-methylacetamide, *N*,*N*-dimethylacetamide, formamide, *N*-methylformamide, and *N*,*N*-dimethylformamide) have been calculated using density functional theory (DFT) and measured using the threshold collision-induced dissociation (TCID) method. For DFT, the combined basis sets of ECP28MWB for silver and 6-311++G(2df,2pd) for the other atoms were found to be optimal using a series of test calculations on Ag^+ binding to methanol and to formamide. In addition, the Ag^+ binding energies of all ligands were evaluated with nine functionals after full geometric optimizations. TCID binding energies were measured using a triple quadrupole mass spectrometer. Reasonable to good agreements were obtained between the calculated and experimental silver(I) binding energies. Ligation of Ag^+ to the alcohols was primarily via the oxygen, although *n*-propanol and *n*-butanol exhibited additional, bidentate coordination via the C—H hydrogens. By contrast, silver(I) binding to the amides was all monodentate via the carbonyl oxygen. There appears to be strong correlations between the binding energies and the polarizabilities of the ligands.

Introduction

The silver(I) ion has 46 electrons with a closed-shell structure of $4s^24p^64d^{10}$. The bioinorganic chemistry of this ion is diverse and interesting; some silver complexes have remarkable antimicrobial activities. For example, the silver ion has long been applied as a bactericide in eye drops used on newborns.[1−4] The metallothioneins, a class of small proteins involved in metal transport and detoxification in mammals, exhibit very high affinities for Ag^+.[5−7] Furthermore, silver(I) binds strongly to peptides in the gas phase;[8−10] sequencing of argentinated peptides, produced via electrospray or matrix-assisted laser desorption/ionization, and identifying the proteins from which they originate, have been demonstrated to be effective.[11−13]

Recent density functional theory (DFT) examinations have shown that Ag^+ can be mono-, di-, or tricoordinate in complexes with α-amino acids;[14] tetracoordinated Ag^+ has been postulated for relatively small peptides.[14] The binding of silver(I) to glycine, di- and triglycine, and to a number of other polypeptides has been investigated.[15] In particular, the structures of argentinated glycine and its oligomers have been examined in detail by means of DFT.[15] The structures were found to fall into three major categories: (a) five-membered cyclic structures in which the silver ion is dicoordinated by the amino nitrogen and the carbonyl oxygen atoms, (b) multiple ring structures in which the silver ion is chelated by three or four atoms, and (c) silver salts in which the silver ion is bound to the carboxylate anion of the zwitterionic amino acid or peptide. Structures from categories a and b have been described as "charge-solvated" as the amino acid or peptide effectively solvates the silver ion in the gas phase; category c complexes are "salt-bridge" structures.

The binding energy between Ag^+ and a ligand, L, is the enthalpy change, $\Delta H°_T$, of the following dissociation reaction at temperature *T*, typically 0 K.

$$Ag^+{-}L \rightarrow Ag^+ + L$$

By contrast, the silver ion affinity (SIA) of L is defined as the binding energy at 298 K. The relative SIAs of the α amino acids have been measured by means of the Cooks' kinetic method.[16,17] A subsequent DFT study verified these measurements, while noting systematic trends for small biases that might have stemmed from differences in the two competing dissociation channels of the $[L{-}Ag{-}L']^+$ complex.[9] Cooks' kinetic method provides *relative* measurements of the binding energies, whereas the threshold collision-induced dissociation (TCID) method affords *absolute* measurements of the binding energies.[18] The Ag^+ and Na^+ binding energies of a number of small oxygen-[19] and nitrogen-containing ligands[20] having been measured using the TCID method. These ligands were selected as models for some of the functional groups in proteins. Within a given homologous series, binding energies increased with the degree of substitution. For the oxygen-containing ligands, the silver ion binding energies were larger than the corresponding sodium ion binding energies[21] but were smaller than lithium ion binding energies.[19,22] This trend was also found for the nitrogen-containing ligands but was more pronounced for the amines and was attributed to the preference of Ag^+ for the softer nitrogen rather than the harder oxygen atom.[19]

Very recently, infrared multiphoton dissociation (IRMPD) spectroscopy has been applied to probe the structures of gas-phase ions, including those of argentinated amino acids.[23−25] These findings have largely substantiated many of the structures predicted by DFT.[9,11] A feature in all of these structures is Ag^+

* To whom correspondence should be addressed. Phone: (416)650-8021. Fax: (416)736-5936. E-mail: kwmsiu@yorku.ca.
† York University.
‡ MDS Analytical Technologies.

10.1021/jp8055653 CCC: $40.75
Published on Web 10/08/2008

binding via the carbonyl oxygen of the carboxyl (amino acids) and amide (peptides) groups. To model Ag^+ binding to peptides, especially in terms of the accuracy of the binding energies, we decided to systematically examine using DFT calculations and TCID measurements the silver ion binding energies to two series of amides: (a) formamide, *N*-methylformamide, and *N*,*N*-dimethylformamide; and (b) acetamide, *N*-methylacetamide, and *N*,*N*-dimethylacetamide. To determine the adequacy of the levels of theory used, the binding energies of the two smallest systems, $[Ag(CH_3OH)]^+$ and $[Ag(HCONH_2)]^+$, were calculated using a wide variety of functionals (27 in all) each with six different basis sets. In a subsequent step, nine independent functionals were used for all silver(I) complexes to calculate the binding energies, which were then compared with the TCID results. As we were performing the experiments on a newer-generation tandem mass spectrometer than the one that we had previously used,[20] we decided for verification purposes to remeasure the binding energies of a series of alcohols and also to expand the study to larger alcohols.[19]

Experimental Method and Data Treatment

Threshold CID measurements were conducted on a PE SCIEX API 365 triple-quadrupole mass spectrometer (Concord, Ontario, Canada) that had previously been modified by having its second quadrupole (q2) replaced by a 20-segment RF-only quadrupole contained in a chamber end-capped with 3-mm diameter ion lenses.[26] The gas pressure/density variation as a function of the position along the *z* axis had previously been studied for effusive conditions, indicating that the effective length is equal to the actual length of the chamber, 20.6 cm.[27−29] The chamber containing the resolving quadrupoles was operated at a base pressure of 5×10^{-6} Torr, as measured by a Bayard−Alpert ionization gauge. Sample solutions were 100 μM in ligand and 40 μM in silver nitrate in 20/80 water/methanol (all chemicals from Sigma-Aldrich, St. Louis, MO). The sample solutions were introduced into the ion source at atmospheric pressure using a syringe pump (Harvard Apparatus, South Natick, MA) at a typical flow rate of 5 μL/min and ionized by means of pneumatically assisted electrospray, using a potential of 5 kV with air being the nebulizer gas. The ions were sampled from the atmospheric pressure ion source under a nitrogen counterflow and into a quadrupole RF ion guide (q0) where multiple collisions with nitrogen, sampled along with the ions, take place at a pressure of 8.5 mTorr as measured using a Baratron absolute capacitance manometer (MKS, type 722A, Andover, MA). The bias potentials in the ion guide and preceding ion optical elements were chosen to strike a compromise between adequate transmission and minimal heating of the silver-ligand complex. Collision-induced dissociation in q2 was performed with argon (Air Liquide Canada Inc., Brampton, Ontario, Canada) as the neutral gas. The gas pressure in q2 was continuously monitored by a Baratron absolute manometer and the flow of the collision gas controlled by a mass flow controller (MKS, type 1179A) coupled to a power supply/readout module (MKS, type 247D) to maintain a stable but variable pressure at 0.02−0.30 mTorr.

Determination of TCID Energies. The threshold energy for the CID of a given Ag^+—L complex was determined using the curve-fitting and modeling program, CRUNCH, developed by Armentrout and co-workers[30−36]

$$\sigma(E) = \sigma_0 \Sigma g_i (E + E_i - E_0)^n / E \qquad (1)$$

where $\sigma(E)$ is the dissociation cross section, σ_0 is a scaling factor, E is the center-of-mass collision energy, E_0 is the threshold energy, E_i is the internal energy of a given vibrational state with a relative population of g_i, and n is an adjustable parameter.

An inherent assumption in the use of eq 1 is that a precursor ion with an internal energy greater than E_0 will fragment to form the product ions in q2. With increasing complexity of the precursor ion, there is an increasing probability that the fragmentation reaction would not occur within the precursor ion's residence time in q2. For a relatively large precursor ion (having many vibrational degrees of freedom), additional internal energy is needed to ensure that the fragmentation rate is sufficiently high for the dissociation to be observable within q2. This additional internal energy, the "kinetic shift", must be subtracted from the apparent threshold to yield the true E_0. The magnitude of this kinetic shift can be estimated from the unimolecular rate constant of the dissociation according to the Rice−Ramsperger−Kassel−Marcus (RRKM) theory.[37−39] When this is done, eq 1 is modified to become

$$\sigma(E) = \sigma_0 \Sigma g_i P(E, E_i, t)(E + E_i - E_0)^n / E \qquad (2)$$

where P is the probability that a precursor ion of collision energy E and internal energy E_i will fragment within a residence time of t.

The residence times of the argentinated complexes were estimated as previously[40] and ranged from 60 to 85 μs. The dissociation cross sections were determined as a function of the center-of-mass collision energies at three collision-gas pressures: 0.05, 0.1, and 0.15 mTorr. As a result of both the short ion path between Q1 and q2 and the low background pressure that remained constant and independent of the pressure in q2, high product ion abundances typically resulted so that no background correction for premature fragmentation was required. Detector/chemical noise, as determined in the first points of the fragmentation curve, was subtracted.

All E_0 values were determined in triplicate over a center-of-mass energy range of 0−4 eV. Experimental binding energies are reported as the standard error of the mean at the 90% confidence level ($t = 2.920$). The kinetic energy distributions of the ions entering q2 were estimated via retarding potential analysis.[30,41] The first-derivative plots of the relative abundance vs the difference in bias potentials between q0 and q2 showed typical full-width-at-half-maximum values of approximately 1.7−2.3 V, thus translating to center-of-mass energy distributions of approximately 0.29−0.51 eV in the threshold CID experiments, which were factored into the determination of $\sigma(E)$. The position of the maximum of the Gaussian distribution indicates the zero point of the energy scale; the deviation from zero applied voltage was used to correct E_0, following literature procedures.[41−43]

The ions used in this study were generated at room temperature and, after supersonic expansion, underwent collisional cooling and focusing in the q0 region.[44] Extensive studies have shown that thermalization of the sampled ions in the q0 region is highly efficient.[44−48] Time-of-flight measurements showed that the average residence time of $[Ag(MeOH)]^+$ ions in q0 was 25.3 ± 1.2 msec. At a gas pressure of 8.5 mTorr and a q0 length of 18 cm, this corresponds to an average velocity of 7.1 m s^{-1}. For a cation of m/z 139, a thermal velocity of 204 m s^{-1} is calculated for 300 K; the motion of thermalized ions in q0 must have been the results of penetration of electric fields via the end-caps, space charge, gas bulk flow, or a combination of these.[45,46] While the ion translational temperature is thermal, the vibrational and rotational temperatures, as well as the extent of RF-heating are less well-known, and will be the subject of a

TABLE 1: Experimental and Theoretical Ag^+/Alcohol Binding Energies (kcal mol^{-1})

			n-C_3H_7OH			n-C_4H_9OH	
ligand	CH_3OH	C_2H_5OH	monodentate	bidentate	i-C_3H_7OH	monodentate	bidentate
E_0[a] (eV)	1.53 ± 0.15	1.67 ± 0.20	1.83 ± 0.20		1.87 ± 0.19	2.04 ± 0.23	
$\Delta H_0°$ (kcal mol^{-1})	35.3 ± 3.4	38.6 ± 4.6	42.3 ± 4.6		43.1 ± 4.4	47.1 ± 5.2	
E_0(PSL)[b] (eV)	1.53 ± 0.14	1.60 ± 0.18	1.63 ± 0.20		1.62 ± 0.17	1.70 ± 0.18	
$\Delta H_0°$ [c] (kcal mol^{-1})	35.3 ± 3.3	36.9 ± 4.1	37.7 ± 4.6		37.4 ± 3.9	39.1 ± 4.2	
B3LYP[d] (kcal mol^{-1})	33.5	37.2	37.2	38.9	39.2	37.7	40.3
average[e] (kcal mol^{-1})	32.6 ± 1.6	36.6 ± 2.0	36.3 ± 1.8	38.1 ± 2.4	38.5 ± 2.0	36.8 ± 1.8	40.1 ± 2.9
	[5.2]	[6.3]	[5.1]	[7.3]	[5.8]	[5.2]	[8.8]

[a] Threshold energy ± standard error of the mean at the 90% confidence level. [b] Threshold energy with correction for kinetic shift. [c] Ag^+ binding energy with correction for kinetic shift. [d] B3LYP/(ECP28MWB + 6-311++G(2df,2pd)). [e] Ag^+ binding energies ± standard deviations calculated using nine DFT functionals with ECP28MWB basis set for Ag and 6−311++G(2df,2pd) basis set for H, C, and O (see Supporting Information for details); values in square brackets are maximum deviations (the largest minus the smallest binding energies).

TABLE 2: Theoretical Ag^+/n-Alkanes Binding Energies (kcal mol^{-1})

	n-C_4H_{10}		n-C_5H_{12}	
ligand	monodentate	bidentate	monodentate	tridentate
B3LYP[a]	19.7	22.6	20.0	25.0
average[b]	19.7 ± 1.4	23.0 ± 2.2	20.1 ± 1.4	25.6 ± 2.7
	[4.9]	[6.8]	[5.0]	[8.4]

[a] B3LYP/(ECP28MWB + 6−311++G(2df,2pd)). [b] Ag^+ binding energies ± standard deviations calculated using nine DFT functionals with ECP28MWB basis set for Ag and 6-311++G(2df,2pd) basis set for H and C (see Supporting Information for details); values in square brackets are maximum deviations (the largest minus the smallest binding energies).

future publication. We are assuming that in this study the ion temperature is 298K because the ions are transferred using the smallest potential gradient possible and under low resolution conditions in Q1 to minimize RF heating. Further experimental and modeling details are available in the Supporting Information section.

Experimental Uncertainties. The sample standard deviation, s_i, of the individual uncertainty contributions ($x_i - x_{av}$) was determined using the contributions of three replicate experiments, according to $s_i = (\Sigma(x_i - x_{av})^2/(3 - 1))^{0.5}$. The total standard deviation of a given E_0 determination is the root-sum-of-squares of the sample standard deviations of all the steps or stages. In Tables 1−3, E_0 (with or without kinetic-shift modeling) is reported with the standard error of the mean at the 90% confidence level ($t = 2.920$).[49−51] Uncertainty in the ion temperature was estimated as follows: [52] by assumption that the ion temperature falls within 298 ± 50 K, the errors in E_0 due to uncertainty in ion temperature were determined by modeling E_0 at three sets of conditions: (a) ion temperature = 298 K (standard), (b) ion temperature = 348 K (high), and (c) ion temperature = 248 K (low). The uncertainty in E_0 became ± 0.03−0.06 eV, depending on the size of the ion. As a result of the TCID data scatter and range of the collision energy, the threshold and RRKM model fits some reactions better than others (see, for example, Figure 1). To take curve-fitting and energy-range errors into account, threshold energies were determined over an E_{cm} range truncated by 1.5 eV (laboratory frame), which were included in Tables 1 and 3. The threshold energies thus obtained differ within ±0.05 eV from the energies obtained without truncating the data set, contributing between 0.01 and 0.25 kcal/mol to the estimated standard deviation. The data scatter for $[Ag(HCONHCH_3)]^+$ and $[Ag(CH_3CON(CH_3)_2)]^+$ is more severe, and a shift in the threshold energy up to 0.07 and 0.14 eV is calculated for the truncated data set. The resulting error contribution (0.5 and 1.18 kcal mol^{-1}) is included in Tables 1 and 3. Similarly, contributions to the sample standard deviation of E_0 from uncertainties in the vibrational frequencies of the precursor ions and products, the flight distance or residence time, the kinetic shift, distribution of the kinetic energies, and the zero-point potential were estimated by determining threshold energies within the error margin of individual factors. As the sample standard deviations for the minimum and maximum absolute values for the uncertainties of the residence time, distribution of kinetic energy, frequency, and temperature are different as a result of the nonlinearity of CRUNCH, a conservative (but statistically not rigorously correct)[53] approach was used by incorporating the *larger* uncertainty for any given factor or stage. Altering the vibrational frequencies of the precursor

TABLE 3: Experimental and Theoretical Ag^+/Amide Binding Energies (kcal mol^{-1})

ligand	$HCONH_2$	$HCONH(CH_3)$	$HCON(CH_3)_2$	CH_3CONH_2	$CH_3CONH(CH_3)$	$CH_3CON(CH_3)_2$
E_0[a] (eV)	1.72 ± 0.17	1.86 ± 0.20	2.29 ± 0.28	1.95 ± 0.16	2.33 ± 0.22	2.75 ± 0.38
$\Delta H_0°$ (kcal mol^{-1})	39.7 ± 4.0	42.9 ± 4.5	52.8 ± 6.5	45.1 ± 3.8	53.8 ± 5.1	63.5 ± 8.7
E_0(PSL)[b] (eV)	1.70 ± 0.18	1.76 ± 0.19	1.91 ± 0.23	1.82 ± 0.15	1.94 ± 0.19	2.07 ± 0.32
$\Delta H_0°$ [c] (kcal mol^{-1})	39.3 ± 4.1	40.7 ± 4.3	44.1 ± 5.4	42.0 ± 3.4	44.7 ± 4.4	47.7 ± 7.5
KM[d] (kcal mol^{-1})	38.7 ± 2.6	42.8 ± 2.6	46.1 ± 2.6	43.3 ± 2.6	47.3 ± 2.6	49.7 ± 2.6
B3LYP[e] (kcal mol^{-1})	43.9	47.3	49.8	47.6	50.4	52.1
average[f] (kcal mol^{-1})	43.2 ± 1.6	46.4 ± 1.8	48.8 ± 1.9	46.9 ± 1.8	49.6 ± 1.9	51.2 ± 2.1
	[5.1]	[5.0]	[5.4]	[4.9]	[5.2]	[5.9]
CCSD(T)[g] (kcal mol^{-1})	41.9	45.7	48.0	45.9	49.0	50.9

[a] Threshold energy ± standard error of the mean at the 90% confidence level. [b] Threshold energy with correction for kinetic shift. [c] Ag^+ binding energy with correction for kinetic shift. [d] Kinetic method results ± standard error of the mean at the 90% confidence level.[75] [e] B3LYP/(ECP28MWB + 6-311++G(2df,2pd)). [f] Ag^+ binding energies ± standard deviations calculated using nine DFT functionals with ECP28MWB basis set for Ag and 6-311++G(2df,2pd) basis set for H, C, N, and O (see Supporting Information for details); values in square brackets are maximum deviations (the largest minus the smallest binding energies). [g] CCSD(T)/[HW(f), 6-31+G(d)].[75]

ions and the products systematically by ±10% resulted in a change of the E_0 by ±(0.01−0.06) eV. The estimated uncertainty in the residence time (between 50 and 200%[54]) resulted in a relatively small error in E_0 of ±0.03 eV. The kinetic shifts on all but one of the ligands examined were within 0.4 eV; we estimated that the maximum error in E_0 as a result of the uncertainty in the kinetic shift was ±0.02 eV. The kinetic-energy distribution's contribution was determined by varying between ±0.5 eV (laboratory frame) and resulted in an uncertainty of ±0.06 eV. The zero-point potential uncertainty based on a range of ±0.15 eV (laboratory frame) was estimated to be ±0.02 eV.

Computational Methods

Determination of E_0 requires the vibrational frequencies and rotational constants of the precursor ions and the transition states. The transition states were assumed to be loose and product-like (the phase-space limit, PSL), and their vibrational frequencies were approximated by those of the neutral products obtained in the DFT calculations. Each transition state was assumed to be variationally located at the centrifugal barrier and the adiabatic 2D rotational energy was calculated using the statistical average approach detailed by Rodgers et al.[35]

Initially DFT calculations, employing Becke's three-parameter hybrid functional formalism (B3LYP), involving Hartree−Fock exchange and Becke's exchange functionals[55,56] and Lee, Yang, and Parr's correlation functional,[57] with the DZVP[58] basis set implemented in Gaussian 03 quantum chemical package,[59] were used to calculate the optimized geometries and vibrational frequencies of the ligands and their silver(I) complexes. All structures were characterized to be at minima by harmonic frequency calculations.

The binding energy between Ag^+ and a ligand, L, $\Delta H_0°$, was then calculated as follows

$$\Delta H_0^\circ = \Delta E_{\text{elec}} + \Delta E_{\text{ZPVE}}$$

where ΔE_{elec} and ΔE_{ZPVE} are the changes in electronic energies and zero-point vibrational energies, respectively, between the products and the reactant in the dissociation reaction.

The effects of basis sets on the computed silver ion binding energy were subsequently explored using the smallest complexes, $[Ag(CH_3OH)]^+$ and $[Ag(HCONH_2)]^+$, as test systems. The initial B3LYP/DZVP geometries were further optimized using 26 additional DFT functionals that included GGA, hybrid, and hybrid meta functionals with the Pople's basis sets for main group elements and the Stuttgart/Dresden relativistic effective core potential basis sets for silver.[60−62] In general, the binding energies increased with increasing size of the basis set for each functional. The difference in the results obtained for the largest basis sets, the quasi-relativistic basis set (ECP28MWB)[60,61] and the relativistic basis set (ECP28MDF),[62] for the silver ion were insignificant. However, the latter is approximately four-fold more time-consuming than the former; we, therefore, used the former in examining all the complexes. Basis set superposition errors (BSSE) were calculated using the full counterpoise correction procedure[63] for some functionals. By use of the basis sets containing two d and one f function for the first-row elements and two p and one d function for hydrogen, the BSSE was negligible with an absolute value of 0.2−0.3 kcal mol^{-1} (∼1% of the binding energy). The BSSE was significantly smaller than the differences in binding energy obtained using different functionals (standard deviation 2−3 kcal mol^{-1}, for details, see Supporting Information). Consequently, for the larger complexes, the ECP28MWB (vide supra) and 6-311++G(2df,2pd) basis sets were used with no BSSE corrections applied. For reporting in this main article, the binding energy for each complex as evaluated using the B3LYP functional is supplied together with an average of the values obtained by nine independent DFT functionals. See the Supporting Information for details.

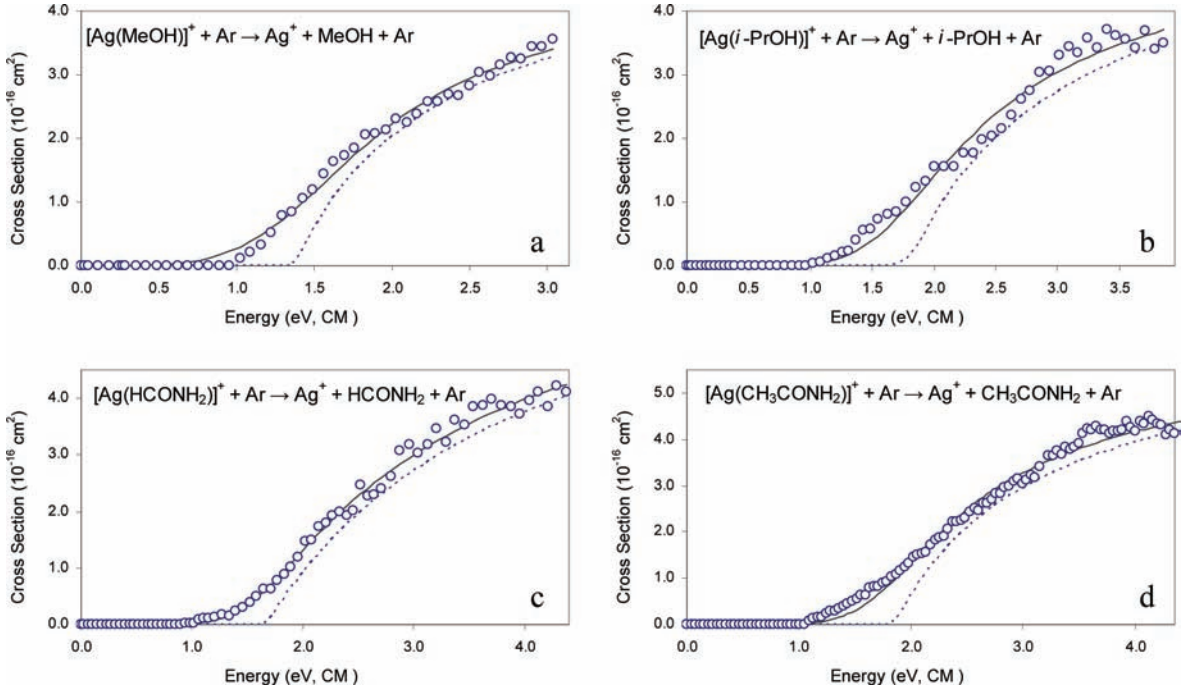

Figure 1. Representative cross sections for CID of (a) $[Ag(CH_3OH)]^+$, (b) $[Ag(CH_3CH(OH)CH_3)]^+$, (c) $[Ag(HCONH_2)]^+$, and (d) $[Ag(CH_3CONH_2)]^+$. Open circles, experimental data; solid lines, best fits to the experimental data; dashed lines, modeled cross sections at 0 K after correction for the kinetic shifts.

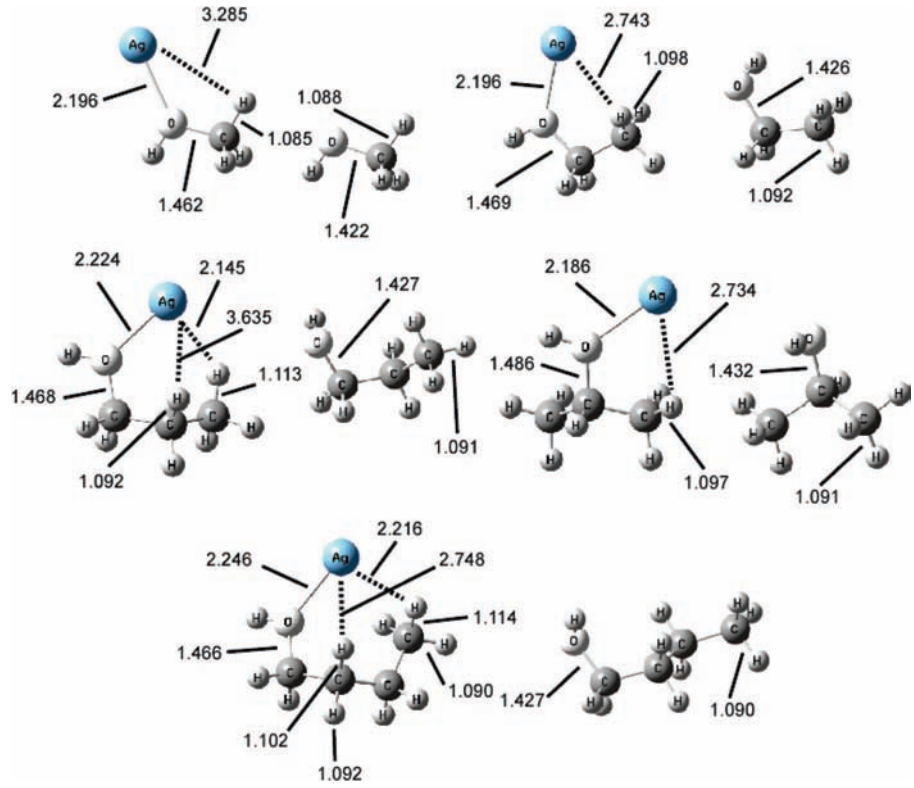

Figure 2. Optimized structures of the alcohols and their argentinated complexes at the B3LYP/(ECP28MWB + 6-311++G(2df,2pd)) level of theory. Interatomic distances are in angstroms.

Results and Discussion

The Alcohols. CID of argentinated alcohols under our experimental conditions produced Ag^+ as the only fragment ion (see panels a and b of Figure 1 for representative cross-section data). The results are summarized in Table 1. Comparison of E_0 data obtained without considering dissociation rates (i.e., no kinetic shifts included, data labeled as E_0) and those with kinetic shifts (labeled as E_0 (PSL)) shows an increasing contribution by the kinetic shift with the size of the ligand, as observed for Li^+/alcohol complexes.[64] Given the uncertainties in our experiments (vide infra), the kinetic shift only becomes significant for the larger alcohols.

The geometries of the argentinated alcohols as calculated using B3LYP/(ECP28MWB + 6-311++G(2df,2pd)) calculation are shown in Figure 2. Eight other functionals were used with the same basis set for geometry optimizations; the resulting structures were not significantly different. For example, the root-mean-square value for the difference of the Ag—O distance calculated at the B3LYP level and with other DFT functionals is only 0.004−0.025 Å. By contrast, the binding energies obtained from the different functionals vary moderately for the complexes, with standard deviations in the range of 1.6−2.9 kcal mol^{-1} and maximum deviations (the differences between the largest and the smallest values for each complex) as large as 8.8 kcal mol^{-1} for $[Ag(n\text{-}C_4H_9OH]^+$. The binding energies evaluated at the B3LYP level and the average values obtained from the nine selected DFT functionals are given in Table 1.

Ag(I) binds primarily to the oxygen with an increasing propensity for additional secondary interactions with the C—H hydrogens with increasing hydrocarbon chain length. In all cases, binding of Ag^+ results in lengthening of the C—O bond (1.462−1.486 Å) relative to that of the free alcohol (1.422−1.432 Å); see Figure 2. The calculated Ag^+ binding energies using the nine DFT functionals and the ECP28MWB + 6-311++G(2df,2pd) basis sets are all comparable within the uncertainties of the experiments and the range of theoretical energies (see Table 1).

The binding energies determined here are within the experimental errors when compared with published data: methanol, 36.3 ± 1.9 kcal mol^{-1};[65] 33.0 ± 7.6 kcal mol^{-1};[19] ethanol, 33.9 ± 7.2 kcal mol^{-1}.[19] No other published data are available, with the exception of a kinetic method study by McLuckey et al.,[66] where the relative silver ion affinities were found to increase with the length of the alcohol side chain and there was a prediction of an upper limit of 7 kcal mol^{-1} difference in the silver ion affinities of methanol and *n*-propanol.

The interaction between the metal ion and the ligand is predominantly electrostatic.[67−70] The increase in binding energy with increasing molecular complexity of the ligand has been rationalized by an increase in ion-induced dipole interaction in the complex,[69,70] a consequence of the increase in polarizability with more extensive substitution.[68,70] The incremental change in Ag^+ binding energy with substitution is uneven, as determined by both experiment and calculation. The experimental uncertainties somewhat mask the trend, which is more apparent in the B3LYP results. The observed increase from methanol to ethanol to *n*-propanol decreases with substitution and agrees with the expected quenching of the inductive effect after the second carbon in the alkyl chain;[71] this trend was also observed in lithium ion affinities.[64] In reality, the increase is larger than what is expected from a pure Ag—O interaction, as some of the increase is attributable to Ag···HC interactions.

Structural evidence for additional interactions is provided by lengthening of the C_4—H bond (1.114 Å, the italicized subscript hereon indicates the carbon number) in *n*-butanol and of the C_3—H bond (1.113 Å) in *n*-propanol. For hydrogens not interacting with the silver, the calculated C—H distances (1.085−1.092 Å) are comparable to those in the free alcohols

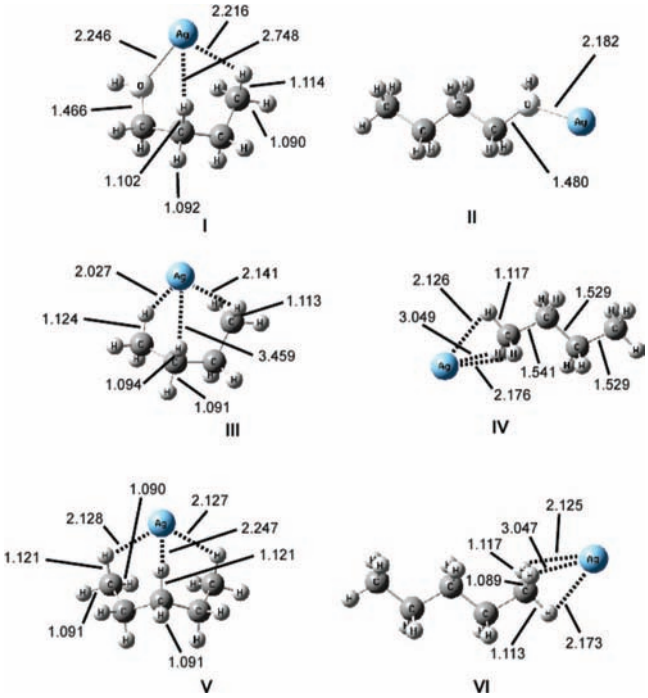

Figure 3. $[Ag(n\text{-}C_4H_9OH)]^+$ (**I**, **II**), $[Ag(n\text{-}C_4H_{10})]^+$ (**III**, **IV**), and $[Ag(n\text{-}C_5H_{12})]^+$ (**V**, **VI**) complexes optimized at B3LYP/(ECP28MWB + 6−311++G(2df,2pd)): **I**, **III**, and **V** are "solvated" structures, while **II**, **IV**, and **VI** are "extended" structures (see the text). Interatomic distances are in angstroms.

(see Figure 3). The shortest Ag···H interatomic distances are 2.216 Å toward the C_4 hydrogen in *n*-butanol and 2.145 Å toward the C_3 hydrogen in *n*-propanol. These interatomic distances qualify the interactions as agostic bonds, for which an interatomic distance of 1.8−2.3 Å and a small metal−H−C bond angle of 90−140° are required (see Supporting Information for details).[72] The strength of the secondary Ag···H interaction was estimated from the difference in binding energies between an optimized "charge-solvated" bidentate structure (Figure 3, structure **I**) and an "extended" monodentate structure (Figure 3, structure **II**) using DFT calculations (see Table 1).

At all levels of theory, an increase in $\Delta H_0°$ is observed for the Ag^+/alcohol structures from $[Ag(CH_3OH)]^+$ to $[Ag(C_2H_5OH)]^+$. In the absence of a charge-solvating geometry, the observed increase in bond dissociation energy is due to the inductive effect.[71] Increasing the hydrocarbon chain length from ethanol to *n*-butanol produces a minimal increase in bond dissociation energy for the *extended* $[Ag(n\text{-alcohol})]^+$ complexes as a result of the decaying inductive effect (Table 1). The observed increase in $\Delta H_0°$ from ethanol to *n*-propanol, therefore, results from the onset of secondary interactions to the latter. Extending the hydrocarbon chain slightly increases this contribution in the case of *n*-butanol.

The contributions of secondary Ag···H interactions in $[Ag(n\text{-alcohol})]^+$ complexes to the $\Delta H_0°$ are modulated by the dominant Ag−O interaction. The weaker Ag···H interactions should be more prominent and apparent in $[Ag(n\text{-alkanes})]^+$ complexes. Consequently, we further investigated these weak interactions in silver(I) complexes with *n*-butane and *n*-pentane using DFT calculations. These results are summarized in Table 2, and all details are given in the Supporting Information. The binding of *n*-butane to Ag^+ was found to be tridentate with a characteristic lengthening of the three C−H bonds for the coordinating hydrogens (see Figure 3). These structural changes are repeated for the Ag^+/*n*-pentane interactions. The difference in the Ag^+ binding energies between the "extended" or monodentate and "solvated" structures in $[Ag(n\text{-}C_4H_{10})]^+$ was found using the B3LYP functional to be 2.9 kcal mol^{-1} and in $[Ag(n\text{-}C_5H_{12})]^+$ 5.0 kcal mol^{-1}. The difference in the gains in Ag^+ binding energies for *n*-butane and *n*-pentane reflects the diminishing steric hindrance toward solvation by hydrogens on different carbons. According to these calculations, C−H hydrogens coordinating to Ag^+ can contribute a total of 2.9−5.0 kcal mol^{-1} in the absence of an electron-donating hydroxyl oxygen, thereby supporting the conclusion that secondary interactions contribute toward the larger Ag^+ binding energies in $[Ag(n\text{-alcohol})]^+$ complexes containing larger alcohols.

The Amides. Only loss of the neutral amide ligand from $[Ag(amide)]^+$ complexes was observed in the CID (see panels c and d of Figure 1 for representative cross-section data). The results are summarized in Table 3. As observed for the alcohols, comparison of E_0 with E_0(PSL) shows kinetic shifts becoming more significant for the larger amides. Minimal differences were observed in the geometries of optimized silver-amide complexes determined using different DFT functionals.

All amide ligands investigated prefer to bind silver(I) through the carbonyl oxygen (see Figure 4). The bidentate binding mode was found to yield less stable complexes that either reverted to monodentate forms during geometry optimizations or gave local high-energy minima on the potential energy surfaces. As a result of transferring electron density from O to Ag, the C−O bond distance increases from 1.216−1.222 Å in the free acetamides to 1.255−1.269 Å in the corresponding silver complexes; a similar behavior is observed in the formamides (see Figure 4). Concurrently, the C−N bond develops more double-bond character and shortens from 1.360−1.370 Å in the free acetamides to 1.323−1.326 Å in the complexes. The calculated Ag−O interatomic distance decreases with increasing N substitution, i.e., as the amino group becomes a more powerful electron donor.

Electron donation affects the amide group polarizability.[70,73,74] Substitution of either an N−H hydrogen or a C−H hydrogen by a methyl group increases the polarizability of the amide, makes the oxygen more basic, and leads to a stronger interaction between silver(I) and the oxygen. Comparisons of the binding energies between isomers $HCONH(CH_3)$ and CH_3CONH_2, as well as $HCON(CH_3)_2$ and $CH_3CONH(CH_3)$ show substitution on the carbonyl carbon increases the silver ion affinity more than substitution on the nitrogen. A linear dependence of the silver(I) binding energy of substituted acetamides and formamides on amide polarizability is observed (Figure 5). A similar dependence is shown for the *n*-alcohols.

A comparison of the experimental and theoretical Ag^+ binding energies obtained using B3LYP/(ECP28MWB + 6-311++G(2df,2pd)) shows good agreement in the order, although the experimental values are systematically lower than the calculated ones. This order is supported by binding energies for Ag^+/amide[75] and Li^+/amide[76] complexes determined using the kinetic method and high-level ab initio calculations at the CCSD(T) level. Within the formamide series, increasing nitrogen substitution increases silver(I) binding energy. From formamide to methyl- and to dimethylformamide, E_0(PSL) increases from 39.3 to 40.7 and to 44.1 kcal mol^{-1}. DFT calculations reproduce this trend (see Table 3). This increase is also observed in replacement of the hydrogen on the carbonyl group by a methyl group. There is reasonable agreement between published Ag^+ binding energies determined using the kinetic method[75] and the Ag^+ binding energies determined here in this study.

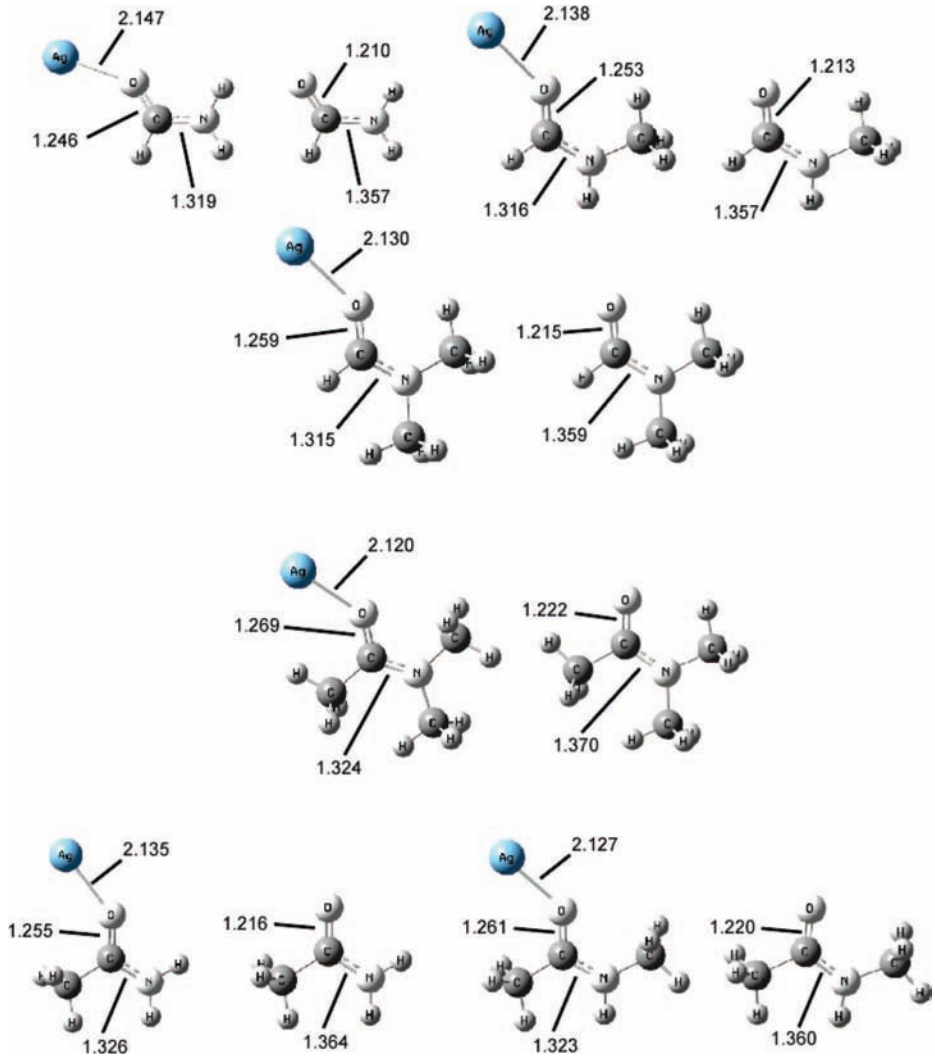

Figure 4. Optimized structures of the acetamides, formamides, and their argentinated complexes at the B3LYP/(ECP28MWB + 6-311++G(2df,2pd)) level of theory. Interatomic distances are in angstroms.

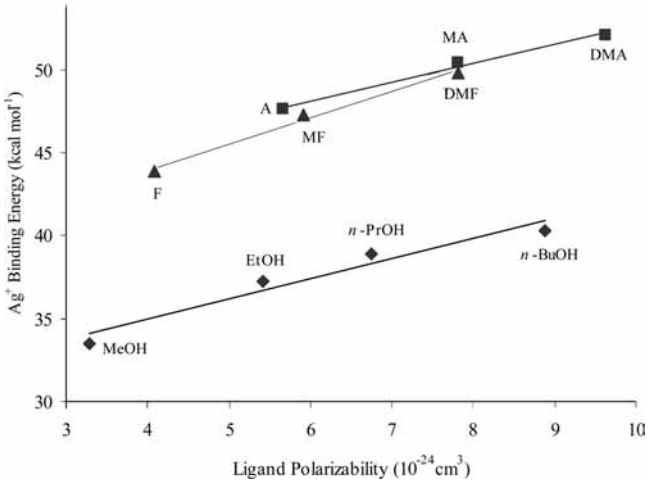

Figure 5. Correlation of the Ag^+ binding energies (as determined with B3LYP, see Tables 1 and 3) for formamides (▲), acetamides (■), and *n*-alcohols (♦) with ligand polarizibility.[73,74] The lines are least-squares fits. Abbreviations used: A, acetamide; MA, *N*-methylacetamide; DMA, *N*,*N*-dimethylacetamide; F, formamide; MF, *N*-methylformamide; DMF, *N*,*N*-dimethylformamide; MeOH, methanol; EtOH, ethanol; *n*-PrOH, *n*-propanol; *n*-BuOH, *n*-butanol.

The uncertainties in the experimental Ag^+ binding energies determined here are two to three times larger than those obtained using a guided ion beam mass spectrometer.[65] While this will make a direct comparison of the data of limited validity, trends in the data are readily discernible. The limitations in using triple quadrupole mass spectrometers for TCID measurements have been discussed[68,77−79] and are related to perturbation of the ion's kinetic energy distribution (RF heating), to limited collection of ions in the collision cell, as well as to uncertainty in the ion's internal energy. Investigations of the various contributions indicate that the major contributor is the uncertainty in the ion temperature, which we have set at 298 ± 50 K. While this choice is somewhat arbitrary, thermalization due to collisions in q0 is highly efficient (see Supporting Information), and this concept has been extensively used in mass spectrometry and physics.[80−85] We will report on the efficiency of collisional cooling in q0, and the contribution of RF heating in Q1, in a future publication.

Conclusions

The silver(I) binding energies of a series of complexes containing either an *n*-alcohol or an amide have been studied by high-level DFT calculations and TCID measurements. The Ag^+ binding energy of alcohols is modulated by a rapidly diminishing inductive contribution and concurrent developing secondary interactions between Ag^+ and the hydrocarbon backbone. The decreasing inductive contribution is only partially compensated by the developing secondary interactions where

the hydrocarbon chain is extended, resulting in a diminishing return in binding energy from ethanol to *n*-propanol. Only monodentate binding occurs in the Ag^+/amide complexes.

Acknowledgment. We thank Peter B. Armentrout for making the CRUNCH program available to us. This work was supported by the Natural Sciences and Engineering Research Council (NSERC) of Canada and MDS Analytical Technologies. V.R. thanks the Ontario Graduate Scholarship in Science and Technology for financial support. Computations in this work were made possible by the facilities of the Shared Hierarchical Academic Research Computing Network (www.sharcnet.ca).

Supporting Information Available: TCID details, experimental uncertainties, experimental parameters, single collision conditions, calculated binding energies with different DFT functionals and basis sets, vibrational frequencies, geometries, and rotational constants. These materials are available free of charge via the Internet at http://pubs.acs.org.

References and Notes

(1) Nomiya, K.; Onoue, K. I.; Kondoh, Y.; Kasuga, N. C.; Nagano, H.; Oda, M.; Sakuma, S. *Polyhedron* **1995**, *14*, 1359–1367.
(2) Nomiya, K.; Kondoh, Y.; Nagano, H.; Oda, M. *J. Chem. Soc., Chem. Commun.* **1995**, 1679–1680.
(3) Franke, S. In *Molecular Microbiology of Heavy Metals*; Nies, D. H.; Silver, S., Eds.; Springer: Heidelberg, 2007, Vol. 6, pp 343−355.
(4) Silver, S. *FEMS Microbiol. Rev.* **2003**, *27*, 341–353.
(5) Gui, Z.; Green, A. R.; Kasrai, M.; Bancroft, G. M.; Stillman, M. J. *Inorg. Chem.* **1996**, *35*, 6520–6529.
(6) Stillman, M. J.; Presta, A.; Gui, Z.; Jiang, D.-T. In *Metal-Based Drugs*; Gielen, M., Ed.; Freundv: London, 1994; Vol. 1, pp 375−393.
(7) Narula, S. S.; Mehra, R. K.; Winge, D. R.; Armitage, I. M. *J. Am. Chem. Soc.* **1991**, *113*, 9354–9358.
(8) Li, H.; Siu, K. W. M.; Guevremont, R.; Le Blanc, J. C. Y. *J. Am. Soc. Mass Spectrom.* **1997**, *8*, 781–792.
(9) Shoeib, T.; Siu, K.W. M.; Hopkinson, A. C. *J. Phys. Chem. A* **2002**, *106*, 6121–6128.
(10) Barr, J. M.; Van Stipdonk, M. J. *Rapid Commun. Mass Spectrom.* **2002**, *16*, 566–578.
(11) Shoeib, T.; Cunje, A.; Hopkinson, A. C.; Siu, K. W. M. *J. Am. Soc. Mass Spectrom.* **2002**, *13*, 408–416.
(12) Chu, I. K.; Guo, X.; Lau, T.-C.; Siu, K. W. M. *Anal. Chem.* **1999**, *71*, 2364–2372.
(13) Chu, I. K.; Cox, D. M.; Guo, X.; Kireeva, I.; McDermott, J. C.; Siu, K. W. M. *Anal. Chem.* **2002**, *74*, 2072–2082.
(14) Chu, I. K.; Shoeib, T.; Guo, X.; Rodriquez, C. F.; Lau, T.-C.; Hopkinson, A. C.; Siu, K. W. M. *J. Am. Soc. Mass Spectrom.* **2001**, *12*, 163–175.
(15) Shoeib, T.; Rodriquez, C. F.; Siu, K. W. M.; Hopkinson, A. C. *Phys. Chem. Chem. Phys.* **2001**, *3*, 853–861.
(16) Brodbelt-Lustig, J. S.; Cooks, R. G. *Talanta* **1989**, *36*, 255–260.
(17) Lee, V. W.-M.; Li, H.; Lau, T.-C.; Guevremont, R.; Siu, K. W. M. *J. Am. Soc. Mass Spectrom.* **1998**, *9*, 760–766.
(18) Armentrout, P. B. *Top. Curr. Chem.* **2003**, *225*, 233–262.
(19) El Aribi, H.; Rodriquez, C. F.; Shoeib, T.; Ling, Y.; Hopkinson, A. C.; Siu, K. W. M. *J. Phys. Chem. A* **2002**, *106*, 2908–2914.
(20) El Aribi, H.; Rodriquez, C. F.; Shoeib, T.; Ling, Y.; Hopkinson, A. C.; Siu, K. W. M. *J. Phys. Chem. A* **2002**, *106*, 8798–8805.
(21) Armentrout, P. B.; Rodgers, M. T. *J. Phys. Chem. A* **2000**, *104*, 2238–2247.
(22) Rodgers, M. T.; Armentrout, P. B. *Int. J. Mass Spectrom.* **2007**, *267*, 167–182.
(23) Forbes, M. W.; Bush, M. F.; Polfer, N. C.; Oomens, J.; Dunbar, R. C.; Williams, E. R.; Jockusch, R. A. *J. Phys. Chem. A* **2007**, *111*, 11759–11770.
(24) Polfer, N. C.; Oomens, J.; Moore, D. V.; Von Helden, G.; Meijer, G.; Dunbar, R. C. *J. Am. Chem. Soc.* **2006**, *128*, 517–525.
(25) Polfer, N. C.; Oomens, J.; Dunbar, R. C. *Phys. Chem. Chem. Phys.* **2006**, *8*, 2744–2751.
(26) Guo, Y.; Siu, K. W. M.; Baranov, V. I. *J. Am. Soc. Mass Spectrom.* **2005**, *16*, 957–966.
(27) Wagenaar, R. W.; de Heer, F. J. *J. Phys. B: At. Mol. Phys.* **1985**, *18*, 2021–2038.
(28) Mathur, B. P.; Field, J. E.; Colgate, S. O. *Phys. Rev. A.* **1975**, *11*, 830–833.
(29) Howard, W. M. *Phys. Fluids* **1961**, *4*, 521–524.
(30) Ervin, K. M.; Armentrout, P. B. *J. Chem. Phys.* **1985**, *83*, 166–189.
(31) Weber, M. E.; Elkind, J. L.; Armentrout, P. B. *J. Chem. Phys.* **1986**, *84*, 1521–1529.
(32) Schultz, R. H.; Crellin, K. C.; Armentrout, P. B. *J. Am. Chem. Soc.* **1991**, *113*, 8590–8601.
(33) Dalleska, N. F.; Honma, K.; Sunderlin, L. S.; Armentrout, P. B. *J. Am. Chem. Soc.* **1994**, *116*, 3519–3528.
(34) Shvartsburg, A. A.; Ervin, K. M.; Frederick, J. H. *J. Chem. Phys.* **1996**, *104*, 8458–8469.
(35) Rodgers, M. T.; Ervin, K. M.; Armentrout, P. B. *J. Chem. Phys.* **1997**, *106*, 4499–4508.
(36) Rodgers, M. T.; Armentrout, P. B. *J. Chem. Phys.* **1998**, *109*, 1787–1800.
(37) Gilbert, R. G.; Smith, S. C. *Theory of Unimolecular and Recombination Reactions*; Blackwell Scientific Publications: Oxford, UK, 1990.
(38) Truhlar, D. G.; Garrett, B. C.; Klippenstein, S. J. *J. Phys. Chem.* **1996**, *100*, 12771–12800.
(39) Holbrook, K. A.; Pilling, M. J.; Robertson, S. H. *Unimolecular Reactions*, 2nd ed.; Wiley & Sons: New York, 1996.
(40) Klassen, J. S.; Kebarle, P. *J. Am. Chem. Soc.* **1997**, *119*, 6552–6563.
(41) Teloy, E.; Gerlich, D. *Chem. Phys.* **1974**, *4*, 417–427.
(42) Gerlich, D. *Adv. Chem. Phys.* **1992**, *82*, 1–176.
(43) Armentrout, P. B. *J. Am. Soc. Mass Spectrom.* **2002**, *13*, 419–434.
(44) Douglas, D. J.; French, J. B. *J. Am. Chem. Soc. Mass Spectrom.* **1992**, *3*, 398–408.
(45) Tolmachev, A. V.; Chernushevich, I. V.; Dodonov, A. F.; Standing, K. G. *Nucl. Instr. Meth. Phys. Res. B* **1997**, *124*, 112–119.
(46) Krutchinksy, A. N.; Chernushevich, I. V.; Spicer, V. L.; Ens, W.; Standing, K. G. *J. Am. Soc. Mass Spectrom.* **1998**, *9*, 569–579.
(47) Lunney, M. D.; Moore, R. B. *Int. J. Mass Spectrom.* **1999**, *190/191*, 153–160.
(48) Kellerbauer, A.; Kim, T.; Moore, R. B.; Varfalvy, P. *Nucl. Instrum. Meth. Phys. Res. A* **2001**, *469*, 276–285.
(49) Box, G. E. P.; Hunter, W. G.; Hunter, J. S. *Statistics for Experimenters*; Wiley: New York, 1978.
(50) Armentrout, P. B. *J. Am. Soc. Mass Spectrom.* **2000**, *11*, 371–379.
(51) Taylor, B. N.; Kuyatt, C. E. *Guidelines for Evaluating and Expressing the Uncertainty of NIST Measurement Results*; NIST Technical Note 1297, 1994 Edition, http://physics.nist.gov/Pubs/.
(52) El Aribi, H.; Rodriquez, C. F.; Almeida, D. R. P.; Ling, Y.; Mak, W. W.-N.; Hopkinson, A. C.; Siu, K. W. M. *J. Am. Chem. Soc.* **2003**, *125*, 9229–9236.
(53) Ang, A. H. S.; Tang, W. H. *Probability Concepts in Engineering Planning and Design*; Wiley: New York, 1975.
(54) Grushow, A.; Ervin, K. M. *J. Chem. Phys.* **1997**, *106*, 9580–9593.
(55) Becke, A. D. *Phys. Rev.* **1988**, *A38*, 3098–3100.
(56) Becke, A. D. *J. Chem. Phys.* **1993**, *98*, 5648–5652.
(57) Lee, C.; Yang, W.; Parr, R. G. *Phys. Rev.* **1988**, *B37*, 785–789.
(58) Godbout, N.; Salahub, D. R.; Andzelm, J.; Wimmer, E. *Can. J. Chem.* **1992**, *70*, 560–571.
(59) Frisch, M. J.; Trucks, G. W.; Schlegel, H. B.; Scuseria, G. E.; Robb, M. A.; Cheeseman, J. R.; Montgomery, J. A., Jr.; Vreven, T.; Kudin, K. N.; Burant, J. C.; Millam, J. M.; Iyengar, S. S.; Tomasi, J.; Barone, V.; Mennucci, B.; Cossi, M.; Scalmani, G.; Rega, N.; Petersson, G. A.; Nakatsuji, H.; Hada, M.; Ehara, M.; Toyota, K.; Fukuda, R.; Hasegawa, J.; Ishida, M.; Nakajima, T.; Honda, Y.; Kitao, O.; Nakai, H.; Klene, M.; Li, X.; Knox, J. E.; Hratchian, H. P.; Cross, J. B.; Bakken, V.; Adamo, C.; Jaramillo, J.; Gomperts, R.; Stratmann, R. E.; Yazyev, O.; Austin, A. J.; Cammi, R.; Pomelli, C.; Ochterski, J. W.; Ayala, P. Y.; Morokuma, K.; Voth, G. A.; Salvador, P.; Dannenberg, J. J.; Zakrzewski, V. G.; Dapprich, S.; Daniels, A. D.; Strain, M. C.; Farkas, O.; Malick, D. K.; Rabuck, A. D.; Raghavachari, K.; Foresman, J. B.; Ortiz, J. V.; Cui, Q.; Baboul, A. G.; Clifford, S.; Cioslowski, J.; Stefanov, B. B.; Liu, G.; Liashenko, A.; Piskorz, P.; Komaromi, I.; Martin, R. L.; Fox, D. J.; Keith, T.; Al-Laham, M. A.; Peng, C. Y.; Nanayakkara, A.; Challacombe, M.; Gill, P. M. W.; Johnson, B.; Chen, W.; Wong, M. W.; Gonzalez, C.; Pople, J. A. *Gaussian 03*, revision D.01; Gaussian, Inc.: Wallingford, CT, 2004.
(60) Andrae, D.; Haussermann, U.; Dolg, M.; Stoll, H.; Preuss, H. *Theor. Chim. Acta* **1990**, *77*, 123–141.
(61) Martin, J. M. L.; Sundermann, A. *J. Chem. Phys.* **2001**, *114*, 3408–3420.
(62) Figgen, D.; Rauhut, G.; Dolg, M.; Stoll, H. *Chem. Phys.* **2005**, *311*, 227–244.
(63) Boys, S. F.; Bernardi, F. *Mol. Phys.* **1970**, *19*, 553–566.
(64) Rodgers, M. T.; Armentrout, P. B. *J. Phys. Chem. A* **1997**, *101*, 2614–2625.
(65) Koizumi, H.; Larsen, M.; Armentrout, P. B.; Feller, D. *J. Phys. Chem.* **2003**, *107*, 2829–2838.
(66) McLuckey, S. A.; Schoen, A. E.; Cooks, R. G. *J. Am. Chem. Soc.* **1982**, *104*, 848–850.
(67) Deng, H.; Kebarle, P. *J. Phys. Chem. A* **1998**, *102*, 571–579.

(68) Rodgers, M. T.; Armentrout, P. B. *Mass Spectrom. Rev.* **2000**, *19*, 215–247.
(69) Shoeib, T.; Gorelsky, S. I.; Lever, A. B. P.; Siu, K. W. M.; Hopkinson, A. C. *Inorg. Chim. Acta* **2001**, *315*, 236–239.
(70) Widmer-Cooper, A. N.; Lindoy, L. F.; Reimers, J. R. *J. Phys. Chem. A* **2001**, *105*, 6567–6574.
(71) Voronkov, M. G.; Feshin, V. P. *Theor. Exp. Chem.* **1973**, *7*, 366–373.
(72) Brookhart, M.; Green, M. L. H.; Parkin, G. *Proc. Natl. Acad. Sci.* **2007**, *104*, 6908–6914.
(73) Miller, K. J. *J. Am. Chem. Soc.* **1990**, *112*, 8533–8542.
(74) Miller, T. M. Atomic and Molecular Polarizabilities. In *CRC Handbook of Chemistry and Physics*, 81st ed.; Lide, D. R., Ed.; CRC Press: Boca Raton, 2000.
(75) Ng, K. M.; Li, W. K.; Wo, S. K.; Tsang, C. W.; Ma, N. L. *Phys. Chem. Chem. Phys.* **2004**, *6*, 144–153.
(76) Tsang, Y.; Siu, F. M.; Ma, N. L.; Tsang, C. W. *Rapid Commun. Mass Spectrom.* **2002**, *16*, 229–237.
(77) Teloy, E.; Gerlich, D. *Chem. Phys.* **1974**, *4*, 417–427.
(78) Gerlich, D. *Adv. Chem. Phys.* **1992**, *82*, 1–176.
(79) Armentrout, P. B. *J. Am. Soc. Mass Spectrom.* **2002**, *13*, 419–434.
(80) Douglas, D. J.; French, J. B. *J. Am. Soc. Mass Spectrom.* **1992**, *3*, 398–408.
(81) Collings, B. A.; Campbell, J. M.; Mao, D.; Douglas, D. J. *Rapid Commun. Mass Spectrom.* **2001**, *15*, 1777–1795.
(82) Krutchinsky, A. N.; Chernushevich, I. V.; Spicer, V. L.; Ens, W.; Standing, K. G. *J. Am. Soc. Mass Spectrom.* **1989**, *9*, 569–579.
(83) Lunney, M. D.; Moore, R. B. *Int. J. Mass Spectrom.* **1999**, *190/191*, 153–160.
(84) Kellerbauer, A.; Kim, T.; Moore, R. B.; Verfalvy, P. *Nucl. Instrum. Method Physics Res. A* **2001**, *469*, 276–285.
(85) Koslovsky, V.; Fuhrer, K.; Tolmachev, A.; Dodonov, A.; Raznikov, V.; Wollnik, H. *Int. J. Mass Spectrom.* **1998**, *181*, 27–30.

JP8055653